The Open University

Open Research Online

The Open University's repository of research publications
and other research outputs

Plasma jet based *in situ* reduction of copper oxide in direct write printing

Journal Item

How to cite:

Dey, Avishek; Lopez, Arlene; Filipič, Gregor; Jayan, Aditya; Nordlund, Dennis; Koehne, Jessica; Krishnamurthy, Satheesh; Gandhiraman, Ram P. and Meyyappan, M. (2019). Plasma jet based in situ reduction of copper oxide in direct write printing. Journal of Vacuum Science & Technology B, 37(3), article no. 031203.

For guidance on citations see FAQs.

© [not recorded]

Version: Version of Record

Link(s) to article on publisher's website:
http://dx.doi.org/doi:10.1116/1.5087255

Copyright and Moral Rights for the articles on this site are retained by the individual authors and/or other copyright owners. For more information on Open Research Online's data policy on reuse of materials please consult the policies page.

oro.open.ac.uk

Plasma jet based *in situ* reduction of copper oxide in direct write printing

Avishek Dey, Arlene Lopez, Gregor Filipič, Aditya Jayan, Dennis Nordlund, Jessica Koehne, Satheesh Krishnamurthy, Ram P. Gandhiraman, and M. Meyyappan

Citation: Journal of Vacuum Science & Technology B **37**, 031203 (2019); doi: 10.1116/1.5087255
View online: https://doi.org/10.1116/1.5087255
View Table of Contents: https://avs.scitation.org/toc/jvb/37/3
Published by the American Vacuum Society

ARTICLES YOU MAY BE INTERESTED IN

Status and prospects of plasma-assisted atomic layer deposition
Journal of Vacuum Science & Technology A **37**, 030902 (2019); https://doi.org/10.1116/1.5088582

Review Article: Atomic layer deposition of optoelectronic materials
Journal of Vacuum Science & Technology B **37**, 030801 (2019); https://doi.org/10.1116/1.5083692

Practical guides for x-ray photoelectron spectroscopy: First steps in planning, conducting, and reporting XPS measurements
Journal of Vacuum Science & Technology A **37**, 031401 (2019); https://doi.org/10.1116/1.5065501

Mechanism for etching of exfoliated graphene on substrates by low-energy electron irradiation from helium plasma electron sources
Journal of Vacuum Science & Technology A **37**, 021401 (2019); https://doi.org/10.1116/1.5080445

Atomic layer deposition of InN using trimethylindium and ammonia plasma
Journal of Vacuum Science & Technology A **37**, 020926 (2019); https://doi.org/10.1116/1.5079279

Epitaxial growth and strain relaxation studies of $BaTiO_3$ and $BaTiO_3/SrTiO_3$ superlattices grown by MBE on $SrTiO_3$-buffered Si(001) substrate
Journal of Vacuum Science & Technology A **37**, 021510 (2019); https://doi.org/10.1116/1.5082237

AVS Quantum Science
Co-published with AIP Publishing

Coming Soon!

Plasma jet based *in situ* reduction of copper oxide in direct write printing

Avishek Dey,[1,2,a)] Arlene Lopez,[1,a)] Gregor Filipič,[1] Aditya Jayan,[1] Dennis Nordlund,[3] Jessica Koehne,[1] Satheesh Krishnamurthy,[2] Ram P. Gandhiraman,[1] and M. Meyyappan[1]
[1]*NASA Ames Research Center, Moffett Field, California 94035*
[2]*School of Engineering and Innovation, The Open University, Milton Keynes, United Kingdom*
[3]*SLAC National Accelerator Laboratory, Menlo Park, California 94025*

(Received 30 December 2018; accepted 15 March 2019; published 5 April 2019)

Printing of nanostructured films with tailored oxidation state and electronic structure can have far reaching applications in several areas including printable electronics, optoelectronics, solar cells, catalytic conversion, and others. Widely used inkjet/aerosol/screen printing techniques require pre- and postprocessing for enhanced adhesion and tailoring of the chemical state of the thin film. Herein, we demonstrate atmospheric pressure plasma jet printing with unique capability to print and tune *in situ* the electronic properties and surface morphology of nanomaterials. Plasma printing of copper thin films with tailored oxidation state from an inexpensive copper oxide precursor is demonstrated and characterized using x-ray absorption spectroscopy, Raman spectroscopy, and electrical measurements. *Published by the AVS.* https://doi.org/10.1116/1.5087255

I. INTRODUCTION

There has been an increased interest recently in fabricating electronic devices on flexible substrates including plastics, cellulose, textiles, and metal foils. Printing of electronic/optoelectronic devices using colloids faces numerous challenges with the major issue being oxidation of the material to be printed, leading to decreased mobility of the charge carriers. Copper has been of interest for various applications due to its high thermal and electrical conductivity. Nanostructured copper with varying oxidation states from pure metallic to cuprous oxide finds applications in printed electronics, optoelectronics, and catalysis.[1–3] Interconnects in integrated circuits (IC) play a crucial role in deciding the system performance and speed. Printing copper interconnects with controlled morphology, and oxidation state is critical in 3D IC packaging, flexible printed circuit boards, and vertical integration. Oxide-derived copper with nanocrystalline surface shows promising catalytic activity and selectivity compared to metallic copper in electroreduction of CO_2 and CO, reflecting the general trend that nanostructured materials with high surface area and porosity have higher conversion efficiencies.[4,5] Printing of porous metal structures is important in catalysis and they are routinely deposited on polymeric templates and postprocessed to remove polymers for achieving the porous structure, which makes high throughput processing a challenge.

Various printing techniques including inkjet, aerosol jet, and screen printing are currently being explored for printed electronics. The routine postprocessing needed to eliminate the solvent and contaminants and the annealing needed to obtain the desired morphology limit the use of low glass transition temperature plastics and add additional processing steps.[6,7] Screen printing is the most widely used process for planar objects; however, the disadvantages include limited resolution, abundance of organic contaminants, and the need for postprint thermal treatment.[8,9] Thermal spray and laser induced sintering are widely used industrial techniques in various other contexts[10] but do not provide the capability to tailor the oxidation state of the printed material as an *in situ process*. High oxygen concentration, high porosity, and difficulty in controlling the microstructure are serious disadvantages of the thermal spray process. Thus, the above printing technologies lack the capability to simultaneously control the microstructure, morphology, and electronic structure of the printed material. Hence, there is a need for an advanced printing technology that can print materials on a range of substrates including semiconductor wafers, textile, paper, plastics, and other flexible substrates. The plasma jet deposition technique presented here offers unique capability to deposit metals and metal oxides with tailored physical and chemical characteristics. Herein, we show printing of copper from an inexpensive precursor such as copper oxide through *in situ* reduction using hydrogen plasma.

Oxidation state and morphology of printed patterns play a crucial role in any device performance regardless of antenna, interconnect, or battery electrode, as mentioned earlier. Laser sintering and/or annealing is typically used to tailor these characteristics. State of the art printing technologies rely heavily on preprocessing of the ink like capping with polyvinyl pyrrolidone and/or addition of stabilizers. Also, postprocessing becomes challenging if multilayered materials are to be printed. The objective of this paper is to demonstrate a direct write "dry" printing that does not require postprocessing and also provide proof of concept studies to show that the atmospheric pressure plasma jet can be used to tailor the oxidation state and morphology *in situ*, thereby avoiding both ink preprocessing and postprocessing of the printed pattern.

II. EXPERIMENTAL WORK

We used a dielectric barrier discharge plasma jet system, where the plasma is ignited by applying a potential between two electrodes with an inert gas passing through a quartz nozzle[11,12] [Fig. 1(a)]. Helium or argon was used at a flow rate of 2000 sccm (99.998% purity) and mixed at the nozzle

[a)]A. Dey and A. Lopez contributed equally to this work.

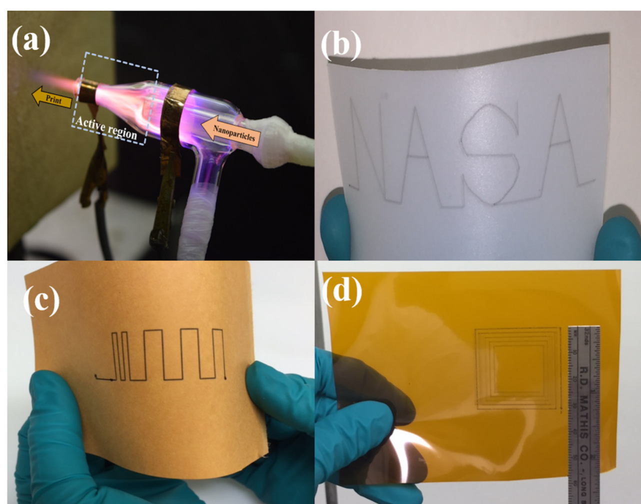

FIG. 1. Photographs of (a) plasma jet printing head, and printing of copper from copper oxide ink on (b) PET and (d) polyimide, and (c) printing of (unreduced) copper oxide using just helium plasma on nanocellulose paper.

with nitrogen (200 sccm) in some cases or hydrogen (25 sccm) for reduction purposes. The plasma is the most intense between the electrodes (active region) followed by the afterglow at the exit of the nozzle.[11,12] Commercially available nozzles used here include Meinhard type C Quartz nebulizer with 0.5 mm capillary (inner diameter) and 5 mm inner diameter Pyrex Sheath Gas Tube (product id: ML116063). The nozzles were designed with two inlets. The inner capillary was used to inject the nanoparticles while the carrier gas was introduced via the outer inlet. Copper tapes wrapped around the glass nozzle act as electrodes (3 cm apart) with one electrode grounded and another connected to a PVM400 model high-voltage AC power supply (Information Unlimited, Amherst, NH) in the range of 1–20 kV and 20–60 kHz frequency. Scaling down the quartz nozzle allows a resolution of 120 μm, and achieving sub-100 μm resolution is possible with smaller nozzles and precise control.

Copper oxide (CuO, Sigma Aldrich) nanoparticles (~50 nm diameter) dispersed in deionized water were used in the printing efforts. The distance between the tip and the substrate influences the film properties such as morphology and uniformity. Here, the tip was kept at a distance of 1 cm from the substrate, which was optimized to get the best results. The microstructure and morphology of the printed samples were studied using Hitachi (Pleasanton, CA) S-4800 field-emission scanning electron microscope (SEM) and Vega 3 Tescan scanning electron microscope at an operating voltage of 10 kV. Current–voltage measurements were carried out with Hewlett-Packard 4155 A Semiconductor Parameter Analyzer with a voltage sweep from −10 mV to 10 mV. The potential was applied across two points separated by 5 mm on the substrate for these measurements.

X-ray absorption spectroscopy (XAS), also referred to as near-edge x-ray absorption fine-structure (NEXAFS) spectroscopy, was performed to understand the surface electronic properties of the printed copper film. Here, a tunable monochromatic source of x-rays with high degree of polarization was used to excite core electrons into unoccupied bound states or continuum states. Cu L-edge and O K-edge NEXAFS measurements were performed at Beamline 8–2 of the Stanford Synchrotron Radiation Lightsource (SSRL), at SLAC National Accelerator Laboratory. For normalization, the incoming flux (I_0) was measured using a gold grid placed in the beam path upstream of the chamber. All samples were mounted on an aluminum stick using a conductive carbon tape and measured under ultrahigh vacuum conditions (<10^{-6} Pa). The drain current from the isolated aluminum stick was used for total electron yield and all measurements were performed at the magic angle of <55° to avoid any potential angular effects. Beamline slits were set to achieve an energy resolution below 0.2 eV (O K-edge) and 0.4 eV (Cu L-edge), respectively. All spectra were first normalized to the incident flux and then subtracted by a linear background, followed by normalization above the edge (atomic normalization).

III. RESULTS AND DISCUSSION

One prominent feature deciding the electron density and temperature of the plasma is the nature of gas used to generate the discharge.[13] The substrate temperature during printing is as low as 35 °C for helium and 50 °C for argon depending on the gas flow rate and applied voltage. The measured substrate temperature for other gas combinations varied from 70 °C to 160 °C in our experiments with maximum temperature observed in the presence of hydrogen. The electron densities (not measured here) in argon and helium are known to be different.[13] The argon plasma has higher electron density than the helium plasma for the same process parameters by about 2.5 times at atmospheric pressure.[14] Thermal conductivity of the gases also varies (1.6×10^{-3} J cm^{-1} s^{-1} K^{-1} for He and 1.8×10^{-4} J cm^{-1} s^{-1} K^{-1} for Ar at 300 K) and as a result, the energy of the plasma varies depending on the nature and type of gases used to generate the discharge. The higher excitation potential of the first excited state for helium (24.5 eV) with respect to that of argon (15.7 eV) results in a much higher electron temperature for helium.[15] However, the gas temperature for argon is higher with respect to helium at the same applied voltage,[16] which is also reflected in the measured substrate temperatures. Most (85%) of the applied energy is lost as heat at the cathode due to Joule heating during plasma generation. Helium is a better heat conductor than Ar; as the gas flow rate increases, the cooling effect becomes more significant, causing the bulk gas temperature to drop significantly for helium. Hence, argon has a higher gas temperature. Introduction of nitrogen and hydrogen with the carrier gas leads to the formation of highly reactive nitrogen and hydrogen species in the plasma.[13] The presence of high-energy metastable states makes it easier to ignite the combination with He.[17] Interaction of these highly active excited species from the plasma with the nanoparticles can potentially alter their chemical and electronic states as well. The momentum of the particles reaching the substrate to form the coating varies depending on various factors including the gas flow rate, nature and the type of gases, applied voltage, size and shape of the nozzle, and the distance between the substrate and the plasma jet. One known major

issue with common inkjet printing process is matching the surface energy of the substrate and the surface tension of the ink leading to a well-known coffee ring effect.[18] Plasmas have often been used to increase the surface energy of substrates which can induce better adhesion of the printed material.[19] A recent study by Wang *et al*. revealed that He plasma enhances the hydrophilicity on a PMMA substrate.[20] Thus, based on the above evidences, the surface energy of the substrate in our system is expected to be adjusted intrinsically, resulting in better adhesion of the printed nanoparticles with the substrate.

Copper was printed on a range of substrates such as polyethylene terephthalate (PET), polyimide, and glass from copper oxide ink (see Fig. 1). Figure 2 shows SEM images of nanoparticle films printed from copper oxide ink using different plasma conditions on silicon [Figs. 2(a)–2(e)] and aluminum substrates [Fig. 2(f)]. We rastered (X-Y stage) the jet over the substrate (1 cm by 1 cm) to achieve a film covering the entire substrate and have taken the images at the center of the substrate. Nanoparticles with the aid of the He plasma retain their shape and do not undergo any physical deformation to a significant extent, as evident in Fig. 2(a). The particles are agglomerated but are mostly spherical similar to the as-synthesized nanoparticles. Introduction of nitrogen into the helium plasma is expected to increase the electron density, electron temperature, and the current density. As shown in Fig. 2(b), the smaller particles undergo partial physical deformation while the larger nanoparticles retain the shape to a certain extent resulting in film formation with particles embedded on it. Figures 2(c) and 2(d) show the results using Ar plasma; as the ion density and gas temperature are higher in this case, the nanoparticles undergo physical deformation resulting in uniform film formation. The melting point of nanoparticles is significantly lower than that of the corresponding bulk materials, a fact known as melting-point depression. The nanoparticle ink used here has average particle size <30 nm and thus, *partial* melting of the nanoparticles is witnessed. These fluidic nanospheres tend to aggregate after reaching the substrate to reduce the surface energy forming a thin film. The surface morphology of the film in this case varied from porous to completely planar in this case.

Figures 2(e) and 2(f) show the film deposited on silicon and aluminum substrates, respectively, using a combination of He, N_2, and H_2. The presence of highly reactive and reducing gases (atomic hydrogen, for example) in the plasma creates a highly porous structure. The formation of systematic pores as shown in Fig. 2(f) is due to the reduced solubility of hydrogen at the solid liquid interface of the copper film and also due to nitrogen. Both aluminum and copper substrates exhibit porosity (copper substrate not shown here) but the porosity is comparatively higher on the aluminum film as shown in Fig. 2(f). This variation in porosity can be linked to the thermal conductivity of the substrates. The temperature at the Al substrate would be much higher, resulting in decreased solubility of hydrogen during the growth of the film. Yamamura *et al.* related the pore formation in copper films to the high hydrogen pressure.[21]

Figure 3 shows the cross-sectional SEM image of the plasma-printed copper film ($\sim 2\,\mu$m thickness) using helium–nitrogen plasma. The adhesion of this film on the glass substrate was checked using a peel off testing and no apparent loss of material was observed. Figure 3 confirms that the thickness of the copper film can be controlled using the plasma process to obtain a dense network without having to anneal at high temperatures. Thus, it is possible to control the morphology, porosity, thickness, and surface roughness

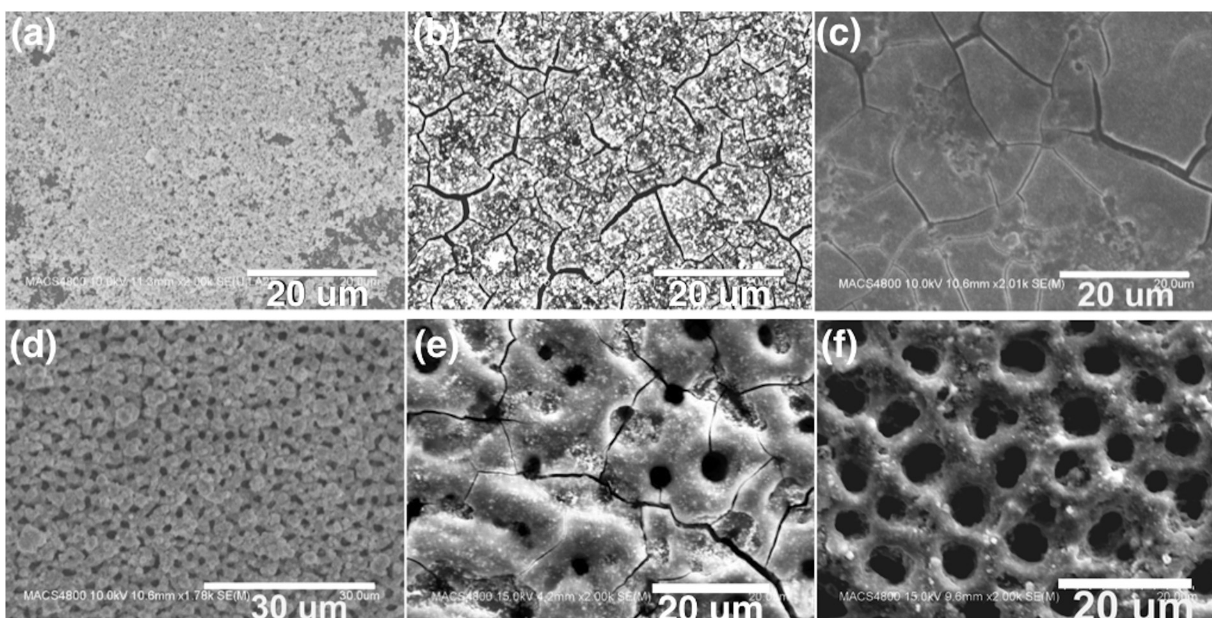

FIG. 2. SEM images of plasma-printed nanoparticles using various plasmas on silicon substrate: (a) helium; (b) helium–nitrogen; (c) and (d) argon; (e) helium–nitrogen–hydrogen showing two different patterns within the same region; and (f) helium–nitrogen–hydrogen on aluminum substrate.

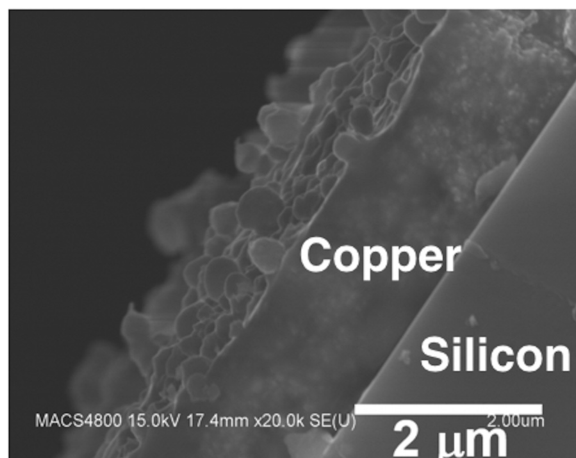

FIG. 3. Cross-sectional SEM image of copper nanoparticle film deposited on silicon substrate showing dense packing.

of the particles/film by carefully controlling the gas mixtures, plasma density, operating voltage, and the distance between the electrode and the substrate.

X-ray absorption spectroscopy (XAS) was performed to gain insight into the electronic state of the printed films. XAS has been widely used to probe into the density of unoccupied states of various materials. It is highly sensitive toward changes in the electronic state or chemical environment of an atom.[22] The estimated depth of electron yield for metals is less than 5 nm, making it an extremely surface sensitive technique. Copper exists in valence states of Cu^{2+} or Cu^{1+} related to cupric and cuprous oxide. The electronic configurations for the states Cu^0, Cu^{1+}, and Cu^{2+} are $(Ar)3d^{10}4s^1$, $(Ar)3d^{10}4s^0$, and $(Ar)3d^94s^0$, where (Ar) denotes the first 18 electrons with configuration same as argon ($1s^2$, $2s^2$, $2p^6$, $3s^2$, $3p^6$). In our discussion here, we will refer to the monovalent and divalent species as d^{10} and d^9, respectively. The electronic and structural properties of Cu-containing compounds have been studied using both Cu *K*-edge and Cu *L*-edge spectra with hard and soft x-rays, respectively.[23,24] The Cu *K*-edge has contribution from multiple final states (3*d*, 4*p*, or 4*s*) at the absorption edge while the Cu *L*-edge consists of a single final state (3*d*) and is easier to interpret.[25] Moreover, the Cu *L*-edge features are sensitive to the valence state of the copper atom and consist of sharp spectral features arising from dipole allowed $2p \rightarrow 3d$ transitions.[26] Here, we studied the Cu $L_{2,3}$ XAS spectra for changes in its oxidation state. The L_3 absorption feature is the outcome of the transition of a core electron from Cu $2p_{3/2}$ to $3d^9$ unoccupied orbital while the L_2 edge is due to Cu $2p_{1/2}$ to $3d^9$ transitions. Yang *et al.* reported that the presence of a strong absorption peak at a photon energy around 931 eV is due to L_3 transitions of divalent copper species.[26] With the reduction of Cu^{2+} to Cu^{1+}, another peak emerges around 934 eV resulting from Cu $2p_{3/2} \rightarrow 3d^{10}4s$ transitions.[27] Though the ground state is predominantly d^{10} configuration, there can be a coexistence of d^9s as well in much smaller amounts.[28]

Figure 4 shows the overlaid XAS spectra of copper films deposited using three different plasma conditions. The

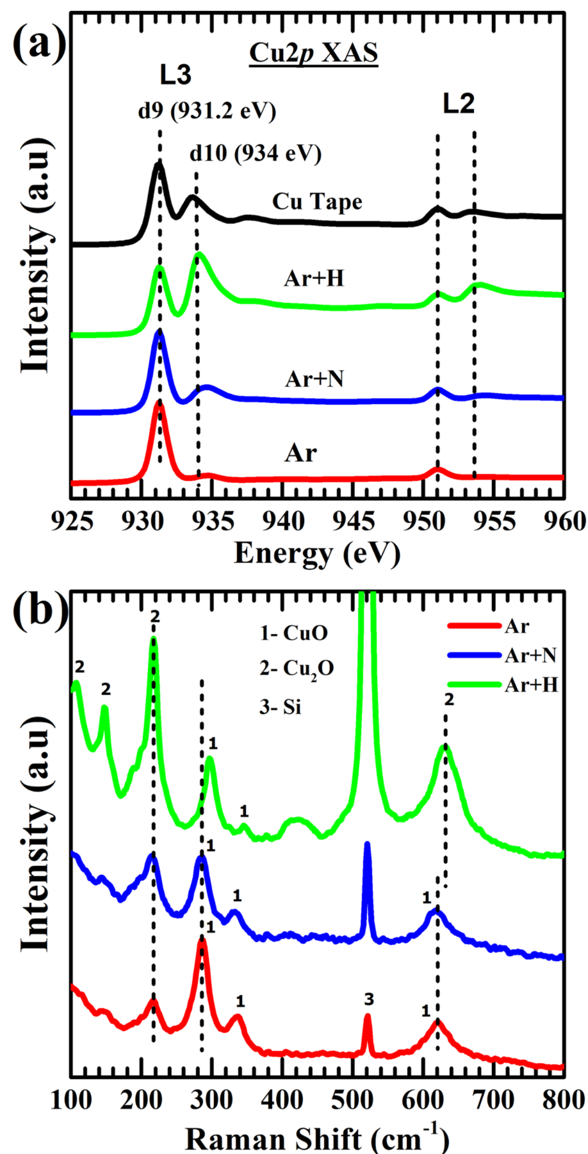

FIG. 4. (a) Cu $L_{2,3}$-edge and O K-edge XAS spectra of printed copper films in total electron yield mode. (b) Raman spectra of the printed copper films.

printing process was carried out using argon and gas mixtures of argon/nitrogen as well as argon/hydrogen for reducing capability. All the spectra were normalized with respect to d^9 at 931.2 eV.[27] The argon-printed sample shows a single sharp feature of $2p \rightarrow 3d^9$ unoccupied orbital transition, indicating a strong presence of Cu^{2+} species. With the introduction of nitrogen and hydrogen, the presence of reduced states is evident from the plot. The intense d^{10} feature for Ar/H_2 printed samples reflects the fact that the presence of excited hydrogen species in the plasma reduces *in situ* to copper nanoparticles. The XAS cross section for d^{10} ($2p \rightarrow 4s$) transitions is considerably smaller (~25 times) than d^9 ($2p \rightarrow 3d$) features. Hence, even a very small concentration of Cu^{2+} species can result in an intense XAS peak. So, it will not be a good approximation to correlate these two peaks to the surface concentration of the valence states. Also, the d^{10} peak is notably broader than d^9 due to hybridization between the final states (3*d* and 4*s* orbitals). However,

the contribution of Cu^0 cannot be neglected as well.[29] These XAS results thus confirm the ability to tailor the electronic properties of copper nanoparticles *in situ* without the need for any post-thermal processing. Regardless of the presence of surface contaminants, the variation in absorption of copper core level is evident for tuning of the oxidation state of the plasma-printed copper film.

Figure 4(b) shows the Raman spectra of the plasma jet printed samples mentioned above. The spectra for all the three samples were calibrated with respect to the Si peak at 530.9 cm^{-1} (peak 3 in the figure). The argon-printed sample shows the dominant presence of CuO phase characterized by the peaks at 285, 335, and 620 cm^{-1}.[30] The peak at 285 cm^{-1} can be assigned to the A_g mode, while the other two peaks correspond to the B_g phonon modes of the CuO crystal. But the presence of the Cu_2O phase in small proportions is reflected by the weak peak around 218 cm^{-1}. This is one of the Raman forbidden modes for the Cu_2O state, which becomes active due to the breakdown of selection rules.[31] Xu *et al.* observed the Raman peaks becoming sharper with a blue shift upon annealing CuO nanocrystals.[30] They related this phenomenon to the increase in the grain size of the nanoparticles. In comparison with the Ar-printed samples, the other two samples showed an increase in the intensity of the peak around 218 cm^{-1}, with the most intense peak for the Ar + H printed sample. The blue shift for the A_{1g} mode of CuO may be due to the high temperature of the plasma, which resulted in grain growth. The peaks around 109, 146, and 628 cm^{-1} along with the intense 218 cm^{-1} peak reflect the existence of copper in Cu^+ oxidation state in bulk. The optically active T_{2g} phonon mode for Cu_2O, meant to be present around 517 cm^{-1}, seems to be suppressed under the intense Si peak.[32] This Raman analysis of the printed thin films provides a strong evidence of the stated *in situ* reduction process and is in absolute agreement with the x-ray spectroscopic measurements.

The current-voltage characteristics of the samples are shown in Fig. 5, including those for the drop-casted copper colloidal solution and also the deposited aerosolized nanoparticles (without turning on the plasma) both on silicon wafer for the purpose of comparison. Both these samples showed very low conductivity and their resistance values were in the range of ∼100 MΩ. The drop-casted sample showed enhanced conductivity when post-treated with the plasma jet for just 1 min, and the conductivity of this sample was higher than a 4-h annealed sample, where the annealing was carried out in a tube furnace at 500 °C in Ar/H_2 atmosphere. This is an indication of the advantage of the plasma jet processing over the standard thermal techniques. The role of plasma–surface interaction requires detailed studies to gain insight into the actual phenomena though there are several possibilities. The plasma exposure results in partial melting of the nanoparticles creating electrical pathways and hence improving the conductivity. The collision of the high-energy electrons and ions with the nanoparticles may likely create local hot spots; they may also partially reduce CuO to metallic copper and the momentum may deform the nanoparticles. Thus, the plasma can play a crucial role in defining

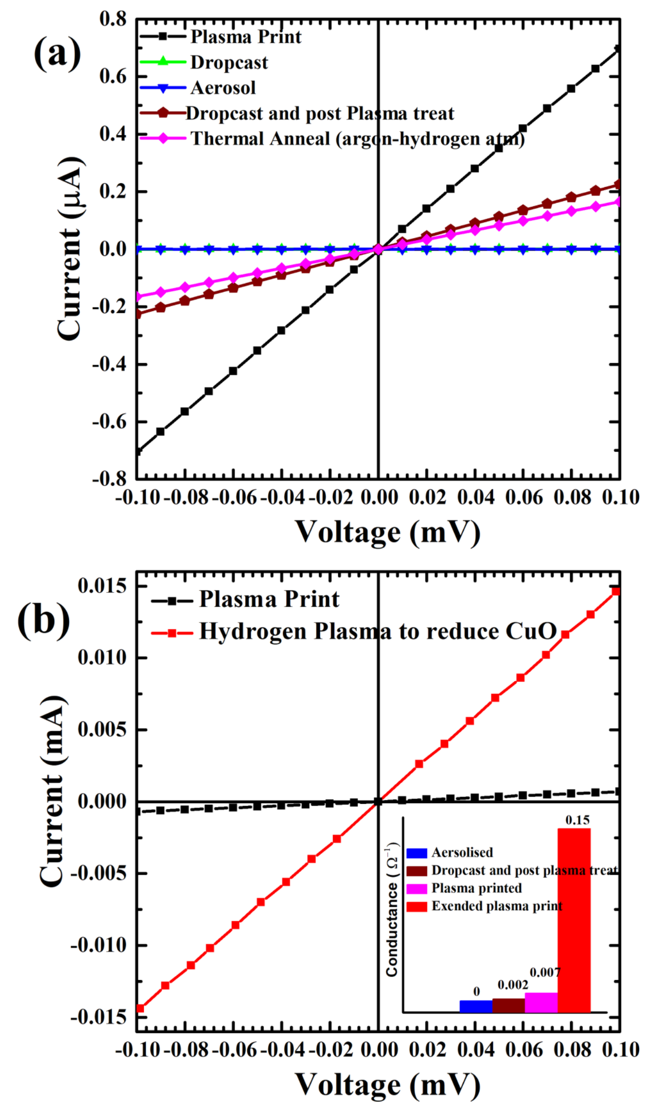

FIG. 5. I–V characteristics of the printed copper film (a) deposited by various methods including plasma printing, drop-casting, and aerosol (b) plasma-printed and plasma-reduced copper film.

the electronic properties of the printed material in addition to gas temperature. The presence of energetic ultraviolet radiation at the effluent of the plasma jet cannot be neglected as well.[33] Hwang *et al.* reported that deep-UV sintering can result in dense packing of the printed nanoparticles.[34]

When the same nanoparticle colloid was printed using Ar/H_2 plasma, it showed a significant rise in conductivity. Although the resistance is of the order of 140 Ω, the rise in conductivity is indicative of the fact that the *in situ* process can be used to create conductive patterns from rather insulating ink. When the printing process was extended with the flow of nanoparticles being cut off, the printed samples showed a drastic drop in resistance. The steep rise in conductance is shown in the inset of Fig. 5(b). Thus, exposing the printed sample to the same plasma jet resulted in ∼20 times decrease in resistance (7 Ω). The increased concentration of metallic copper and a highly connected network may be the principle cause of this phenomenon. One may argue in favor of using other (nonplasma) printing processes and then using

the plasma jet just for a post-treatment to obtain improved conductivity; however, the formation of conductive interconnects within the film will be hard to achieve otherwise. Insets of Figs. 5(a) and 5(b) show the I–V curve and conductance of copper samples drop-casted and post-treated using the plasma jet. It is evident that the conductance of the plasma prints and post-treated samples are 80–100× higher than that of the drop-casted and post-treated sample. Although the conductance values are quite high for the as-synthesized samples, these samples show a considerable deterioration in conductance values over time. This is mainly due to the surface oxidation of the copper nanoparticles when exposed to the ambient.

IV. CONCLUSIONS

The increase in flexible electronics research and applications has attracted much interest in printing of copper nanoparticles and thin films. We have presented here for the first time a direct write printing technology that can tune the electronic property of the printed material *in situ*. The I–V and XAS measurements confirm the ability of the approach to serve as an *in situ* reduction technology in direct write printing and capability to tune the morphology. This system also promotes adhesion to the substrate, uniformity in deposition, and formation of densely packed nanoparticle structure. Desired morphology and electronic structure can be achieved by varying the gases in the plasma. The results affirm plasma jet printing as a promising technology for manufacturing of next-generation printed electronics.

ACKNOWLEDGMENTS

This work was partly funded by the In Space Manufacturing Program of the NASA STMD and NASA Advanced Exploration Systems (AES). A.L. and R.P.G. were employed by the University Space Research Association (USRA) during this work and their work was supported by NASA contract to USRA. A.D. was a visiting Ph.D. student from The Open University, UK and a visiting research scholar with USRA. G.F. was a visiting Fulbright scholar from Jožef Stefan Institute, Slovenia. Use of the Stanford Synchrotron Radiation Lightsource, SLAC National Accelerator Laboratory was supported by the U.S. Department of Energy, Office of Science, and Office of Basic Energy Sciences under Contract No. DE-AC02-76SF00515.

[1]S. H. Ko, H. Pan, C. P. Grigoropoulos, C. K. Luscombe, J. M. J. Fréchet, and D. Poulikakos, Nanotechnology **18**, 345202 (2007).
[2]A. R. Rathmell, S. M. Bergin, Y. L. Hua, Z. Y. Li, and B. J. Wiley, Adv. Mater. **22**, 3558 (2010).
[3]M. B. Gawande, A. Goswami, F.-X. Felpin, T. Asefa, X. Huang, R. Silva, X. Zou, R. Zboril, and R. S. Varma, Chem. Rev. **116**, 3722 (2016).
[4]C. W. Li, J. Ciston, and M. W. Kanan, Nature **508**, 504 (2014).
[5]F. S. Roberts, K. P. Kuhl, and A. Nilsson, Angew. Chem. Int. Ed. **54**, 5179 (2015).
[6]S. Jang, Y. Seo, J. Choi, T. Kim, J. Cho, S. Kim, and D. Kim, Scr. Mater. **62**, 258 (2010).
[7]K. Woo, D. Kim, J. S. Kim, S. Lim, and J. Moon, Langmuir **25**, 429 (2009).
[8]C. Campos-Cuerva, M. Zieba, V. Sebastian, G. Martínez, J. Sese, S. Irusta, V. Contamina, M. Arruebo, and J. Santamaria, Nanotechnology **27**, 95702 (2016).
[9]Y. Kim, B. Lee, S. Yang, I. Byun, I. Jeong, and S. M. Cho, Curr. Appl. Phys. **12**, 473 (2012).
[10]T. Donnelly and J. G. Lunney, Appl. Surf. Sci. **282**, 133 (2013).
[11]R. P. Gandhiraman, E. Singh, D. C. Diaz-Cartagena, D. Nordlund, J. Koehne, and M. Meyyappan, Appl. Phys. Lett. **108**, 123103 (2016).
[12]R. P. Gandhiraman, V. Jayan, J. W. Han, B. Chen, J. E. Koehne, and M. Meyyappan, ACS Appl. Mater. Interfaces **6**, 20860 (2014).
[13]M. A. Lieberman and A. L. Lichtenberg, *Principles of Plasma Discharges and Material Processing*, 2nd ed. (Wiley, Hoboken, NJ, 2005).
[14]M. Moravej, X. Yang, G. R. Nowling, J. P. Chang, R. F. Hicks, and S. E. Babayan, J. Appl. Phys. **96**, 7011 (2004).
[15]J. Jonkers, M. Van de San, A. Sola, A. Gamero, and J. Van der Mullen, Plasma Sources Sci. Technol. **12**, 30 (2002).
[16]Q. Wang, F. Doll, V. M. Donnelly, D. J. Economou, N. Sadeghi, and G. F. Franz, J. Phys. D Appl. Phys. **40**, 4202 (2007).
[17]X.-J. Shao, N. Jiang, G.-J. Zhang, and Z. Cao, Appl. Phys. Lett. **101**, 253509 (2012).
[18]P. J. Yunker, T. Still, M. A. Lohr, and A. G. Yodh, Nature **476**, 308 (2011).
[19]F. Khelifa, S. Ershov, Y. Habibi, R. Snyders, and P. Dubois, Chem. Rev. **116**, 3975 (2016).
[20]R. Wang, Y. Shen, C. Zhang, P. Yan, and T. Shao, Appl. Surf. Sci. **367**, 401 (2016).
[21]S. Yamamura, H. Shiota, K. Murakami, and H. Nakajima, Mater. Sci. Eng. A **318**, 137 (2001).
[22]G. Hahner, Chem. Soc. Rev. **35**, 1244 (2006).
[23]S. J. George, M. D. Lowery, E. I. Solomon, and S. P. Cramer, J. Am. Chem. Soc. **115**, 2968 (1993).
[24]L. Kau, D. J. Spira-Solomon, J. E. Penner-Hahn, K. O. Hodgson, and E. I. Solomon, J. Am. Chem. Soc. **109**, 6433 (1987).
[25]K. Shimizu, H. Maeshima, H. Yoshida, A. Satsuma, and T. Hattori, T. Phys. Chem. Chem. Phys. **3**, 862 (2001).
[26]J. Yang *et al.*, Anal. Chem. **83**, 7856 (2011).
[27]M. Grioni *et al.*, Phys. Rev. B **39**, 1541 (1989).
[28]M. Grioni, J. F. Van Acker, M. T. Czyayk, and J. C. Fuggle, Phys. Rev. B **45**, 3309 (1992).
[29]C. I. Pearce, R. A. D. Pattrick, D. J. Vaughan, C. M. B. Henderson, and G. van der Laan, Geochim. Cosmochim. Acta **70**, 4635 (2006).
[30]J. F. Xu, W. Ji, Z. X. Shen, S. H. Tang, X. R. Ye, D. Z. Jia, and X. Q. Xin, J. Solid State Chem. **147**, 516 (1999).
[31]L. Debbichi, M. C. Marco de Lucas, J. F. Pierson, and P. Krüger, J. Phys. Chem. C **116**, 10232 (2012).
[32]Y. Liu *et al.*, Appl. Phys. Lett. **106**, 123901 (2015).
[33]S. Reuter, K. Niemi, V. Schulz-von der Gathen, and H. F. Döbele, Plasma Sources Sci. Technol. **18**, 15006 (2008).
[34]H.-J. Hwang, K.-H. Oh, and H.-S. Kim, Sci. Rep. **6**, 19696 (2016).